International Master Course in Nanotechnologies and Quantum Devices

INTERNSHIP REPORT

FABRICATION AND CHARACTERIZATION OF DOUBLE ALIGNED MOIRÉ SUPERLATTICES

Supervisors
Dr. Rebeca RIBEIRO-PALAU (C2N)
Prof. Carlo RICCIARDI

Candidate
Gaia MAFFIONE

A.Y. 2021-2022

Acknowledgements

First of all, I'd like to acknowledge the facilities of the Centre de Nanosciences et de Nanotechnologies and the Renatech platform, without which carrying out this project would not have been possible.
I would like to express my deepest gratitude to my supervisor Rebeca Ribeiro-Palau for the work we have done together in the last four months and for teaching me more stuff in such a short period of time than I could ever have imagined. I also must thank all the members of the Topo2D team for always being present during my internship, both as friends and as colleagues, for helping me on my project and for the moments shared in front of a beer or a coffee.
A special mention goes to Mario for all the advice and for initiating me to the Flash Invaders cult.

I also must mention all the people I have met in this crazy adventure that has been my year in Paris, my friends in Turin that have watched me grow during four years at Politecnico and have endured all the good and bad times always by my side, and my friends in Bari that have now known me for a lifetime but are still able to put up with me somehow. No matter where I am, these places will always feel like home to me.

Lastly there are not enough words to thank my family that has always supported and never doubted me in every single thing I do. All that I achieve in this life is dedicated to you.

Contents

Introduction

2D materials are arguably among the most discussed and researched topics of the last two decades. One of the things that makes them interesting is the possibility of obtaining atomically-thick samples, and what makes them unique for future applications is the electronic band structure.

Graphene is a 2D material formed by an hexagonal array of carbon atoms; it is defined as a gapless semiconductor because its conduction and valence bands meet at specific points in k-space, where they form the so-called Dirac cones. Close to the Dirac point, its electronic dispersion is linear: this means that carriers behave like massless Dirac fermions and consequently have a high mobility, much greater than that of a typical semiconductor.[1,2] For this reason, graphene represents an exciting platform for research on electronics, quantum mechanics phenomena and more.
When different 2D materials, such as graphene, hexagonal boron nitride (hBN), transition metal dichalcogenides (TMDs), are stacked on top of each other, the layers are held together by van der Waals (vdW) interactions; the structure resulting is referred to as van der Waals heterostructure. Materials in the 2D family are characterized by strong covalent bonds in the plane direction, providing stability; on the other hand, interlayer van der Waals forces are weak and much different from selective chemical bonds. This implies that virtually any vertical stacking combination between 2D materials is possible,[3] contrary to epitaxially grown 2DEG.

Van der Waals heterostructures are new artificial materials in which emergence of novel hybrid properties is observed. Such properties can effectively be tailored by tuning parameters of the heterostructure, that is the relative rotation between layers and, of course, the choice of materials.
This opens the way for a new generation of electronic devices with improved performances, based on novel quantum phenomena.

In this internship report I am going to focus on van der Waals heterostructures based on graphene and hexagonal boron nitride: the aim is to study the modified electronic properties of graphene, arising from the interactions with hBN. This is done through the fabrication and characterization of devices that allow to tune and measure the properties of the heterostructure, as will be explained later.
The obtained results are going to be compared to the theory and previous literature.

Chapter 1

Context of the Internship

Here I am going to briefly introduce the objective of my internship and the environment in which it was carried out, along with a theoretical description of the subject.

1.1 C2N - Centre de Nanosciences et de Nanotechnologies

I have conducted this internship in C2N – Centre de Nanosciences et de Nanotechnologies; the C2N is a joint research unit between the CNRS and Université Paris-Saclay, hosting state of the art technological facilities and a clean room of 2900 m^2.
The center develops research in the field of material science, nanophotonics, nanoelectronics, nanobiotechnologies and microsystems, as well as in nanotechnologies. In all these fields, its research activites cover all the range from fundamental to applied science.
The laboratory is organized around 4 scientific departments: Photonics, Materials, Nanoelectronics, Microsystems and Nanobiofluidics.

The Department of Nanoelectronics focuses on understanding and realizing nanoscale phenomena and devices, and on developing integrated nanocircuit architectures. It is composed of 5 research groups, among which the PHYNANO group (PHYsics and technology of NANOstructures and quantum systems) in which I have worked. The group gathers research teams that explore different topics of condensed-matter physics at very small scale, from the most fundamental aspects to applications.
I have taken part in the activities of the TOPO2D team, whose focus is the investigation of fundamental properties of topological states observed in 2D materials. The team fabricates van der Waals heterostructures, based on graphene and hexagonal boron nitride, using innovative sample fabrication techniques with new layer alignment control.
Electronic transport experiments at room temperature and low temperatures are performed to understand the physical origin and how to control topological phases.

Research activities focus on two main axes: Quantum Hall Effect (QHE) in graphene, topological spin and valley currents.

1.2 Objectives of the internship

The general objective of the internship is to investigate the effects of the moiré superlattice in double aligned graphene-hBN heterostructures. In order to accomplish this, the following specific targets need to be seeked out:

- fabrication of dynamically rotatable van der Waals heterostructures;
- observation of the moiré superlattice through AFM measurements on the graphene surface;
- characterization of the electronic transport of the devices at room temperature.

1.3 Graphene and Moiré Superlattice

The object of study of this work is van der Waals heterostructures based on graphene and hBN; hBN was first used for graphene encapsulation, to insulate and protect it from the environment. Furthermore, using hBN as a substrate allows to obtain devices in which carrier mobility is enhanced and extrinsic doping of graphene is reduced, compared to devices made of graphene on SiO_2.[2]
We recall the electronic band structure of pristine graphene, shown in figure 1.1: the touching points of the conduction and the valence bands, called Dirac cones, are highlighted in the figure.

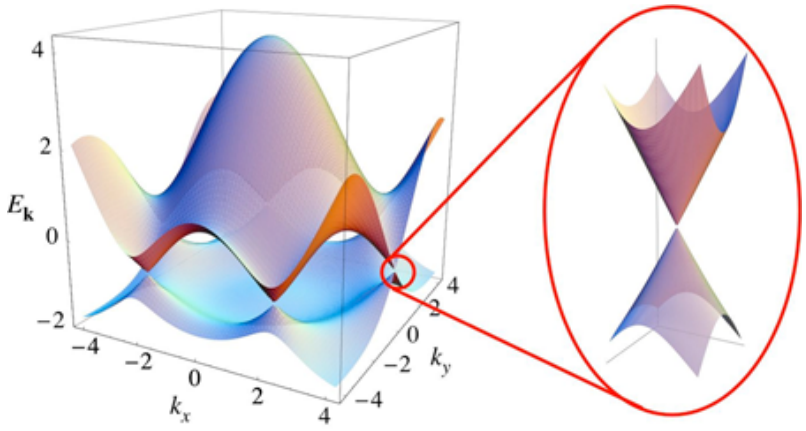

Figure 1.1: Graphene electronic band structure in momentum space. The zoomed inset shows the Dirac cone in one of the K points. Adapted from ref.[4]

Van der Waals heterostructures formed by graphene and hBN become much more interesting when crystallographic alignment is achieved between the layers. In fact, the crystals of both materials are characterized by triangular lattices, where

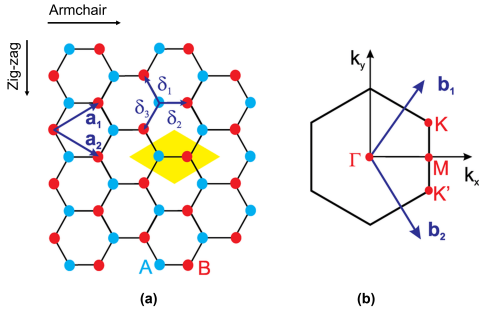

Figure 1.2: (a) Triangular lattice generated by the two vectors $\mathbf{a_1}$ and $\mathbf{a_2}$, the unit cell is highlighted in yellow; the edge types, armchair and zig-zag, are also shown. (b) Triangular reciprocal lattice generated by the two vectors $\mathbf{b_1}$ and $\mathbf{b_2}$.

the atoms are arranged in the shape of a honeycomb as shown in figure 1.2.

The unit cell in real space contains two atoms; in the case of graphene the two atoms are identical carbon atoms, while for hBN one atom is nitrogen and the other one is boron. The lattice constant of graphene is 2.46 Åand in hexagonal boron nitride it is 2.50 Å. This small difference, which makes the hBN lattice 1.8% larger than the one of graphene, allows to obtain a moiré superlattice.

The moiré superlattice consists in a periodic potential that is superimposed to the lattice potential. It can be created artificially by patterning a substrate[5] or naturally by taking two lattices which have the same configuration (e.g. triangular, hexagonal, square).
When two 2D materials with the same lattice structure but different lattice constants are stacked together a moiré pattern forms. The moiré pattern has the same shape as the lattice; its size, namely λ, can be tuned by changing the relative angular alignment of the layers.
This is the case of heterostructures based on monolayer graphene and boron nitride: the largest moiré pattern is observed when the two materials are aligned along the same crystallographic direction, which can be either zig-zag or armchair as reported in figure 1.2. The resulting maximum periodicity is equal to around 14.5 nm,[6] as shown in figure 1.3.

The superimposed periodic potential modifies the electronic band structure of graphene, breaking inversion symmetry and causing the emergence of new Dirac points. The superlattice Dirac points arise at energies which depend on the crystallographic alignment via the periodicity λ, given by:

$$\lambda = \frac{(1+\delta)a}{\sqrt{2(1+\delta)(1-\cos\theta)+\delta^2}} \tag{1.1}$$

where δ is the lattice mismatch bewteen hBN and graphene (0.018), a is the lattice constant of graphene (2.45 Å) and θ is the relative rotation angle between the lattices. The lattice with periodicity λ in real space corresponds to $\mathbf{G}$ vectors in

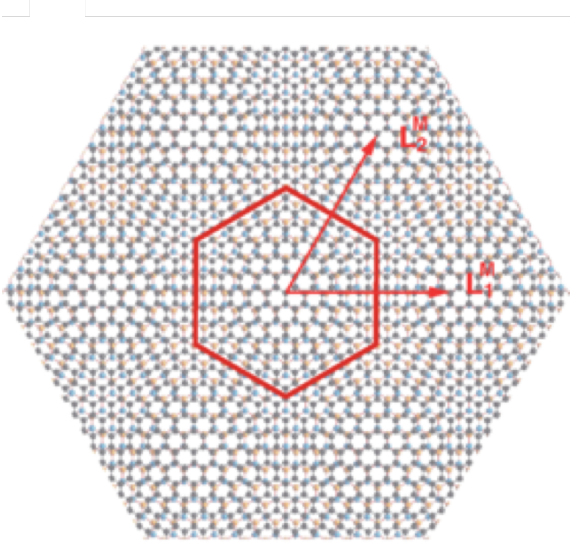

Figure 1.3: Graphene-hBN moiré super-lattice with $\theta = 0$ and an exaggerated lattice constant ratio $a_{\mathrm{hBN}}/a = 10/9$. The red hexagon highlights the unit cell. Adapted from ref.[7]

reciprocal space, given by $\mathbf{G} = \frac{4\pi}{\sqrt{3}\lambda}$.
Using the relation $E = \frac{\hbar v_F |\mathbf{G}|}{2}$ and replacing G with the previous expression, an equation linking the Dirac points to λ can be written as follows:

$$E = \frac{h v_F}{\sqrt{3}\lambda} \tag{1.2}$$

The resulting band stucture can be visualized in figure 1.4: the apperance of the satellite cones is visible both in the conduction and the valence band.

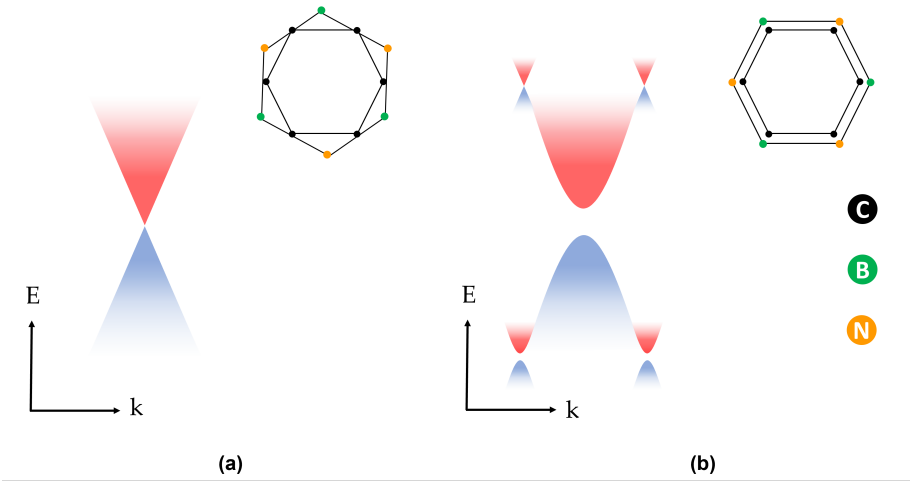

Figure 1.4: Band structure of (a) misaligned heterostructure (equivalent to pristine graphene) and (b) aligned heterostructure.

One rather unexplored aspect of graphene-hBN heterostructures is the case of double alignment, in which the graphene layer is sandwiched between two hBN

layers and all three lattices are aligned. Research conducted so far[8] shows that the moiré potential is effectively enhanced by double alignment, and the graphene couples similarly to both moiré patterns from the top and the bottom BN layers. Very interesting features of double aligned systems are found in the electronic band structure of graphene, whose shape depends on the type of alignment between the boron nitride layers. The vertexes of the hexagons making up the lattice of hBN can either be Boron or Nitrogen atoms; then, if we imagine to stack vertically and align two hBN lattices, the system does not possess 60° symmetry: either two atoms of the same kind overlap, or one B and one N atom. This is precisely the reason why the electronic band structure of graphene aligned to two BN layers is not equivalent upon rotations of 60° of the the top BN flake.
Two different types of band structure have been found: when top and bottom BN layers are aligned so that there is a 0° rotational offset between them, the gaps that appear due to the single graphene-hBN heterostructure are enhanced; on the other hand, if the lattices are rotated by 60° with respect to each other, inversion symmetry is restored. This results in an electronic band structure where the secondary Dirac points are still present, while the gaps at such satellite peaks and at the main Dirac point close, with the conduction and valence bands touching.
These findings are summarized in figure 1.5.

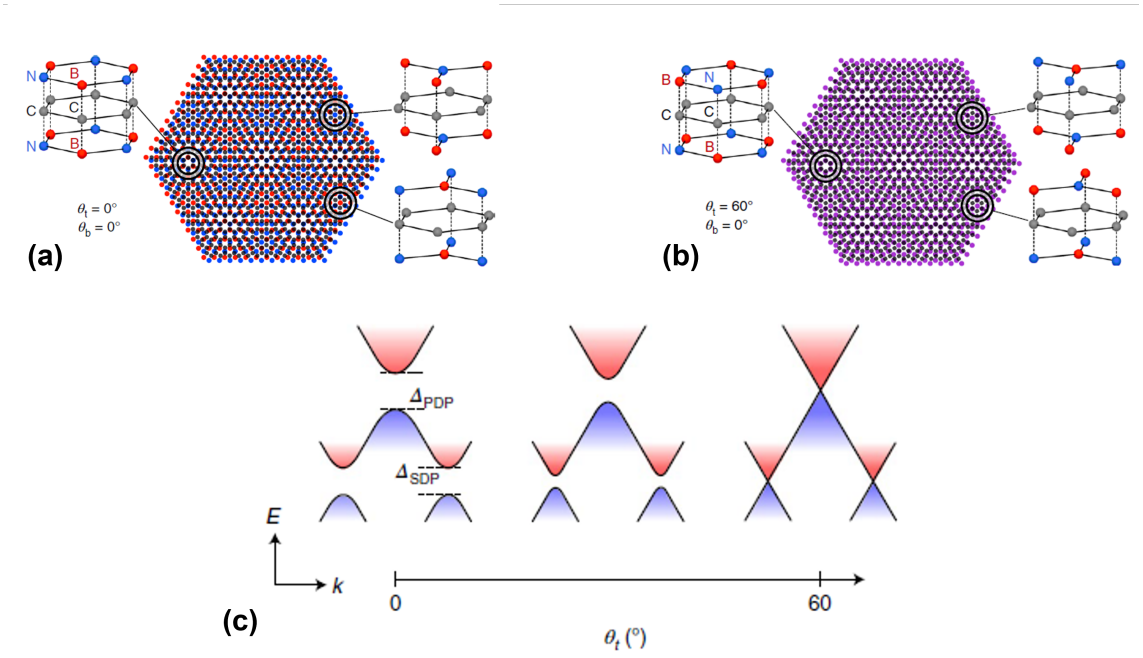

Figure 1.5: Schematics of BN–graphene–BN heterostructures with all layers aligned and 0° (a) or 60° (b) rotational offset between the top and bottom BN layers; lattice models at the high symmetry points of the moiré pattern show the atomic alignment for each. (c) Electronic band structure as a function of the top alignment: 30° corresponds to graphene aligned with a single hBN, 0° shows an enhancement of the gaps and 60° is the case in which inversion symmetry is restores. Adapted from ref.[8]

Chapter 2

Device Fabrication

The process of fabrication of a device requires several different steps, which are briefly illustrated in this chapter. The final structure of the device is schematically shown in figure 2.1. The core of the device is the heterostructure formed by the two hBN layers and graphene; the bottom BN is present also as support to the graphene flake.
The peculiarity of this arrangement is that different alignment angles can be set on a single sample: as the picture shows, an AFM tip is used to rotate the BN handle with respect to graphene. The rotation is performed simultaneously with the electrical measurements, which rely on the bottom graphite gate and the graphene lateral contacts.

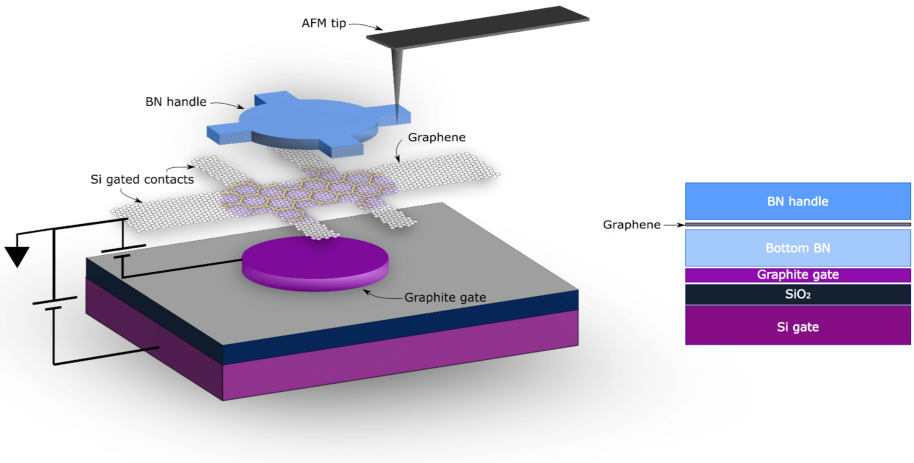

Figure 2.1: (left) Schematics of the dynamically rotatable device, the bottom BN layer has been omitted for clarity. (right) Cross section of the layers. Adapted from ref.[9]

2.1 Exfoliation

There are different ways of producing flakes of 2D materials; a very simple one which also allows to achieve high quality samples is mechanical exfoliation. The steps of

this techniques are summed up in figure 2.2.
Crystals of graphite or hBN are placed on an adhesive tape, which is folded back on itself to reduce the initial thickness of the crystals and spread the material in a bigger area of 1 cm^2. From the initial tape, called *mother-tape*, it is possible to obtain a few *daughter-tapes* by simply placing them on the mother and covering the area where the crystals are.
The tapes can now be placed on diced silicon chips, whose size is 10 x 10 mm; the chips also have a 285 nm thick layer of silicon oxyde SiO_2 grown on the surface.
In the case of graphene only, the chips are also subject to a 15 seconds oxygen plasma treatment to improve the cleanliness by eliminating any organic residues. Afterwards, the tapes are placed on top of the chips which undergo a short baking of about four minutes at 120°C, to improve adhesion. The tapes are then peeled off from the chips, while flakes of the materials will stick to the substrate.
When exfoliating graphene, the tapes are quickly removed to increase the number of flakes on the chip. As for boron nitride, the exfoliation is required to be much slower and gentler.

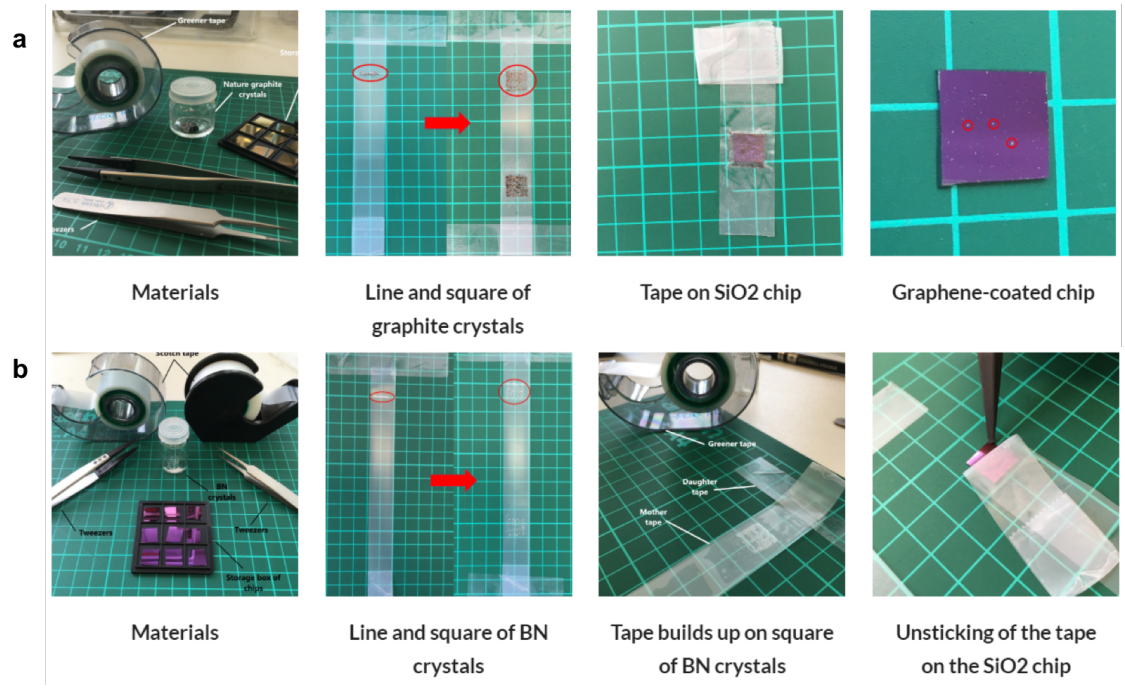

Figure 2.2: Different steps in the exfoliation process of graphite (**a**) and hBN (**b**).

Following exfoliation, it is necessary to check the quality of the flakes using an optical microscope. There are a few criteria for choosing the flakes which can be used to create a heterostructure: size, thickness, homogeneity and cleanliness are the main ones.
The thickness of the flakes can be deduced by the colour, with a certain degree of approximation. Figure 2.3 gives a visual indication of the colour change between flakes of different thickness.
In the case of graphene, the contrast between a monolayer flake and the SiO_2 substrate is not strong, but it can be improved by using a green filter. The green

filter is the optimal choice to maximise the contrast on 285 nm SiO_2 substrates, reaching values around 15%.[10]

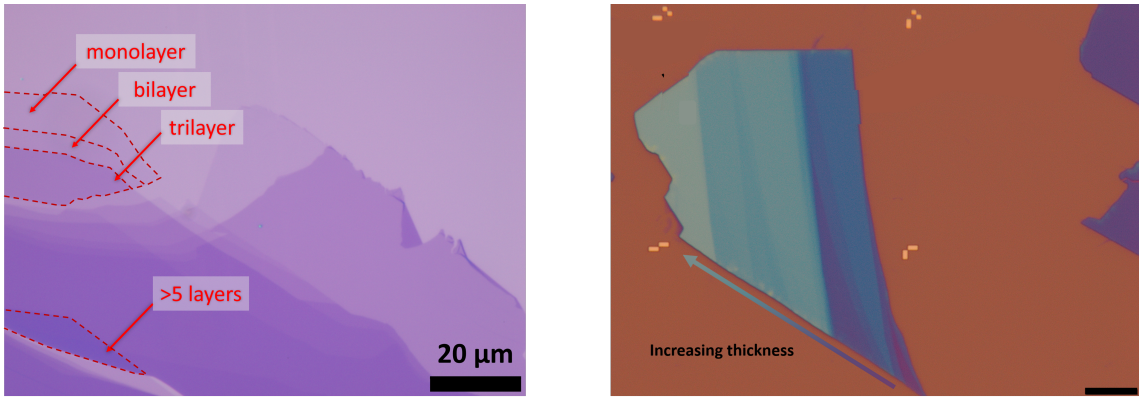

Figure 2.3: (a) Multi-layered graphite flake: it is possible to distinguish areas with 1, 2, 3 and more layers as indicated by the arrows. (b) Multi-layered hBN flake, the scale bar reported corresponds to 10 μm.

Graphene exfoliation provides also thicker flakes of graphite (recognizable by their darker violet/blue colour) which can be used for the fabrication of the bottom gates, as it will be further explained in 2.2.1.
As for BN, it is harder to know the exact thickness of flakes simply by looking at their colour. An accurate estimation of the thickness can be provided by topographic measurements with the AFM.
Nevertheless, it is possible to choose adequate BN flakes by selecting the ones whose colours is in the light blue range, corresponding to the required thickness of around 40 nm.

2.2 Building a van der Waals heterostructure

Once the flakes have been chosen it is possible to proceed with the stacking. The device is built on 5 by 5 mm clean chips patterned with gold alignment marks, which are necessary for future lithography steps.
The different flakes are placed on the chip by dry transfer: each flake can be picked up using polydimethylsiloxane (PDMS) substrates covered by a polymeric film. The polymers used are either polycarbonate (PC) or polypropylene carbonate (PPC),depending on the material to be picked up. In such a way it is possible to pick the materials from the chips in which they were originally exfoliated and deposit them on new ones.
Figure 2.4 briefly shows the steps of picking up a flake with a polymeric film supported by a PDMS cylinder; PDMS also comes in other shapes, i.e. a bubble or a pyramid, for different types of techniques. The steps will be explained in detail in the following sections.

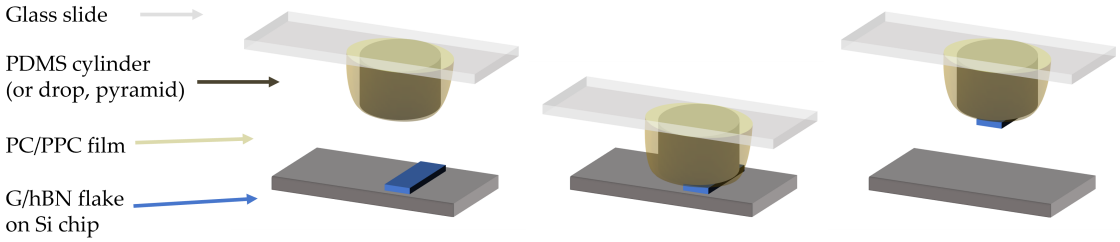

Figure 2.4: Different steps in the pick up process.

As shown in figure 2.1, the aim is stacking vertically different materials (here listed from bottom to the top):

- patterned graphite gate;
- hBN flake, around 40 nm thick;
- monolayer graphene;
- hBN handle.

We want to investigate the properties of a double aligned heterostructure, to do so we need to take care of the alignment of graphene with the bottom hBN flake. Contrary to the handle, in this case the alignment is fixed and is defined during the pick-up process (explained in 2.2.2). In order to align flakes in a static condition, it is required to choose those that present crystallographic edges: such edges are very straight and form an angle which is a multiple of 30°.
During pick-up one has to pay attention to aligning one BN edge to one of graphene. Nevertheless, this doesn't guarantee that alignment has been achieved: a crystallographic edge for an hexagonal lattice may be either *zig-zag* or *armchair* (see figure 1.2), and aligning two of the same kind is necessary to produce the moiré. Unfortunately, it is not possible to predict during flake transfer which kind of edges are being combined as it can only be assessed when measurements are performed on the device. Nonetheless, we decided to characterize not only double aligned devices, but also to investigate those that present single alignment with the top hBN

2.2.1 Patterned graphite gate

The first component to take care of is the bottom gate of the device, which is made of patterned graphite.
Graphite flakes can be picked up using a PDMS bubble, deposited on a glass slide, covered by a PC film; to do so, the substrate holding the film is slowly lowered to contact the silicon chip in the vicinity of the targeted flake. Temperature is increased from 70°C to around 90°C so that the drop-shaped film can expand and stick to the flake. Then, the temperature is slowly lowered back so that the graphite flake is picked up as the film retracts.
The deposition on the marked chip is performed by melting the PC film at 180°C once it is in contact with the substrate. The area chosen for the deposition is near

the central markers and has to be as clean as possible.
The chip is cleaned from the melted polymer by washing in chloroform for a few minutes (5 to 10 minutes); rinsing is then performed in acetone and iso-propyl alcohol (IPA).

A step of electron beam lithography is required to shape the gate into a circle. The deposited graphite is usually exploited to a maximum by designing more than one gate: as many gates as the flake area allows.
Electron beam lithography allows to transfer the designed pattern to the substrate with precision up to 5 nm; the chosen resist is polymethyl methacrylate (PMMA). Samples are spin-coated with 40 g/l solution of PMMA, at 4000 rpm speed. The resist is cured by heating at 170°C for 1 minute.
The PMMA pattern which is exposed to the electron beam is weakened; it is removed by developing with a H_2O:IPA (3:1) solution for 60s, followed by rinsing in IPA. Afterwards the sample is exposed to oxygen plasma etching: this removes the areas of graphite which are no longer covered with the resist, and the pattern is obtained. After the etching is complete, the residual PMMA can be removed from the sample by cleaning in acetone.
A practical example of the result is shown in figure 2.5.

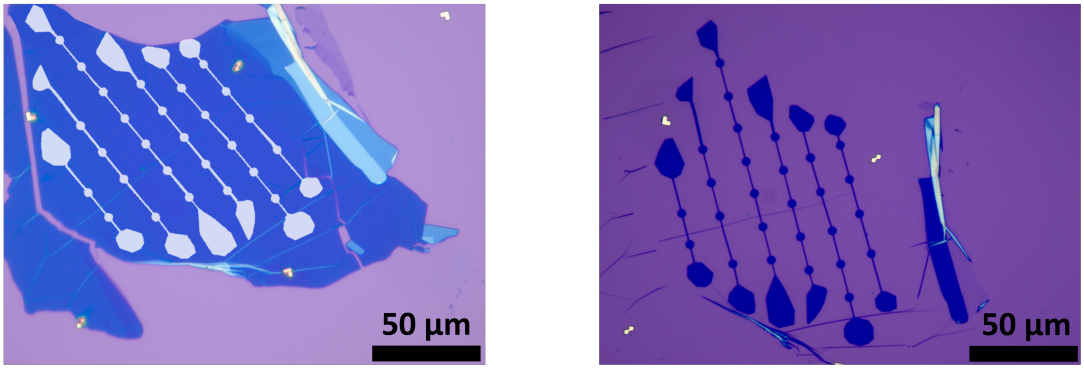

Figure 2.5: (a) Graphite flake deposited on marked chip and pattern (drawn in white) to be obtained. (b) Patterned graphite gates after lithography and etching.

2.2.2 Flip stacks

Building a van der Waals heterostructure with exposed graphene using the dry transfer method is not straightforward: graphene is a delicate material, therefore it is not the first flake to be picked up. The technique used consists in picking up a BN flake first and then picking up graphene with BN, exploiting the van der Waals interactions between the layers.
Figure 2.6 shows the materials used the build a heterostructure and the final result.

Dry transfer steps are performed using a PPC film: the procedure is the same as the one explained for graphite in 2.2.1, except in this case the PPC film is placed

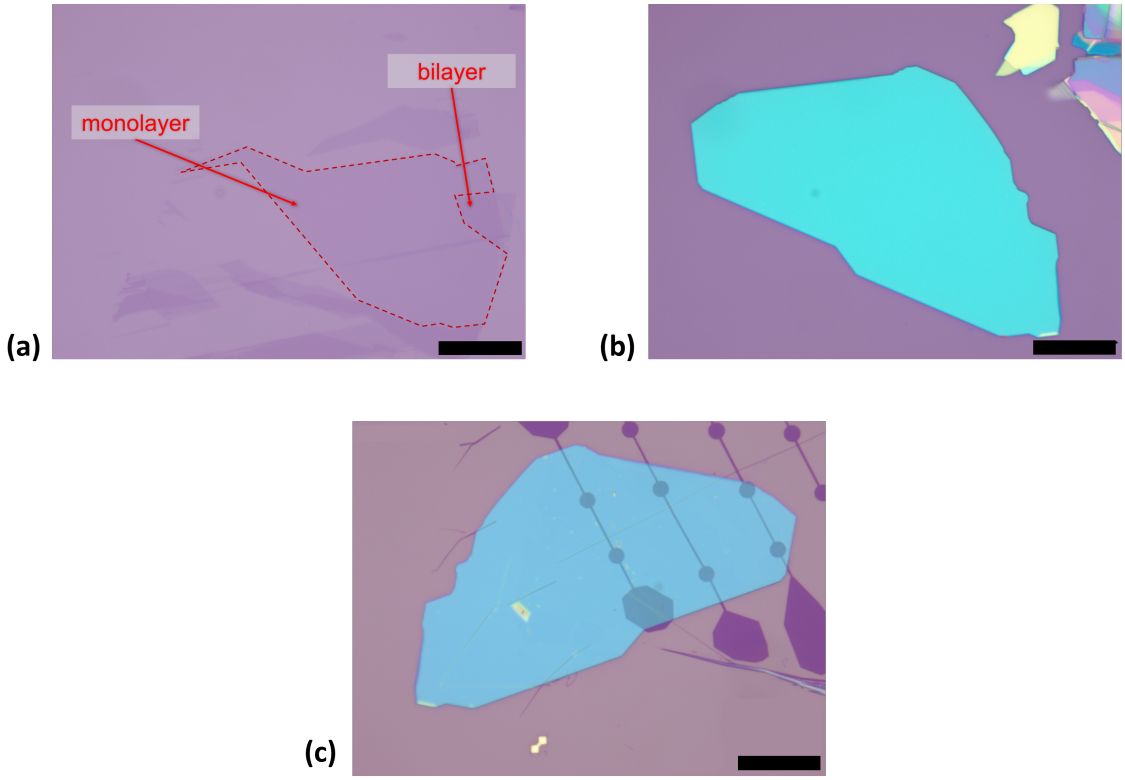

Figure 2.6: (a) Monolayer graphene flake with small bilayer parts (b) BN flake (c) Heterostructure deposited on the gates after flip-stack. Scale bars reported on all images correspond to 20 μm.

on PDMS cylinders and it is heated up to about 45°C to be able to pick up BN. Graphene is picked up at even lower temperatures, around 30°C, simply by covering the flake with the picked BN when the film is put in contact with the substrate. As mentioned, temperature does not really play a role in this process, because it doesn't rely on the adhesive properties on the film: the interactions between BN and graphene alone allow to build the heterostructure.

The stack has to be deposited now on the previously patterned gate: the desired structure is graphite-BN-graphene. This means that it is not possible to simply deposit the heterostructure as it was picked up, because the outcome would have BN on top of graphene.
The right sequence is obtained by doing what is called a *flip-stack*: the PPC film containing the stack is removed from the PDMS substrate and it is flipped; it is then placed on another PDMS bubble in which a hole has previously been made in the center.
It is now possible to proceed with the deposition, by melting the PPC at 180°C; the film should contact the chip at low temperature (20°C), in order to make sure of the correct placement of the heterostructure above the gate area: this can be ensured by checking with the optical microscope. At higher temperatures it is not possible to adjust the position of the film because it will stick on the chip.
Melted PPC is cleaned away from the chip through an annealing treatment at 360°C under vacuum, at a pressure lower than $6 \cdot 10^{-4}$ hPa.

Due to the transparency of graphene, AFM measurements are performed to assess the quality of the heterostructure: it is possible to evaluate the topography by scanning the surface in tapping mode. It is necessary to check that the areas above the circular gates are in good conditions: it is frequent to find cuts or folds due to the stress that the height difference creates upon deposition of the flip stack on the gates.
Figure 2.7 shows two channels on an AFM image taken to check the topography of graphene. The height sensor allows to identify particles deposited on top of the heterostructure, while the phase map is particularly relevant because its different colours indicate different materials. In the picture in question, the graphene flake shows a darker colour; since it shows good quality on the circular gates on the bottom, we can move forward and build devices in these areas.

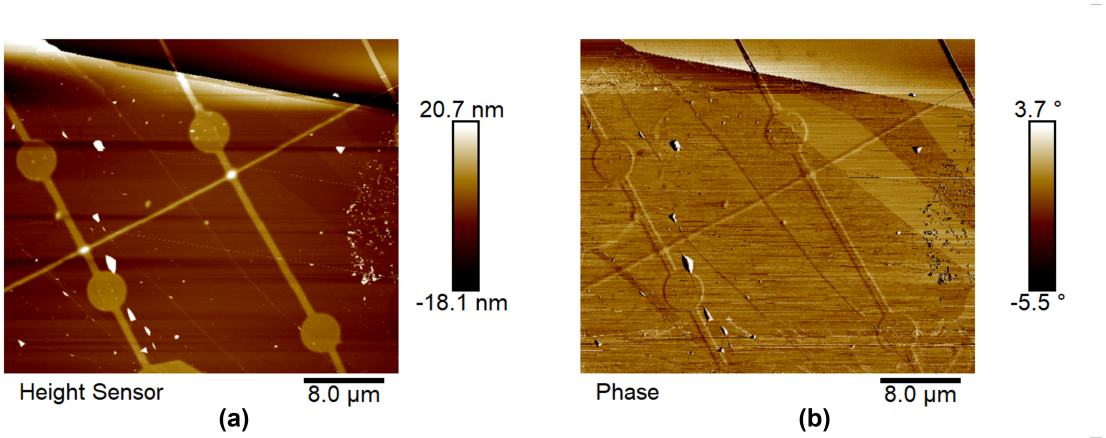

Figure 2.7: (a) Height sensor and (b) phase map of a flip stack after deposition on the patterned gates.

Once acceptable gates have been found, the next step is performing lithography to shape the graphene layer into a Hall-bar, as shown in figure 2.8. This shape allows to perform electrical measurements in the four probe configuration, which will be illustrated in section 4.
Once again the sample is spin coated with PMMA which is exposed to the electron beam; following development of the resist, a short oxygen plasma treatment is performed (about 20 seconds) to pattern graphene.

The handle can now be deposited on top of the Hall bar; BN handles are fabricated by exfoliating Boron-Nitride directly on a marked chip: this allows to perform lithography on such chip. In this case the resist used is hydrogen silsesquioxane (HSQ): when exposed to the electron beam it becomes silicon oxide. It is developed using MF-CD-16 for 15 minutes. After patterning the resist, the exposed BN is etched using CHF_3 and O_2 at 15 mTorr and 10 W of Power. The final result is a patterned hBN layer covered by about 150nm of HSQ.
A handle can be picked up using a PPC film placed on a PDMS pyramid-shaped substrate: the only difference with the previously illustrated PPC dry transfer method is that the contact point of the pyramid with the substrate is much

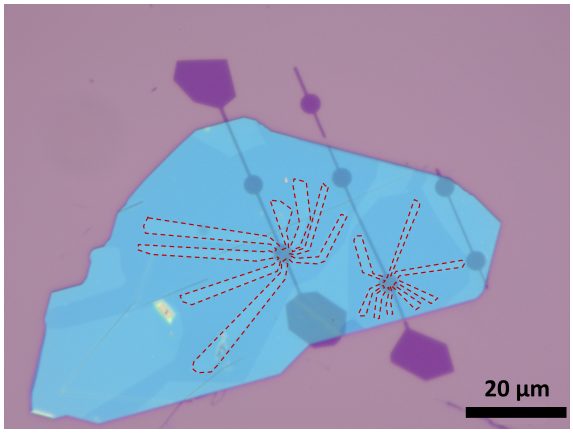

Figure 2.8: Patterned graphene on boron nitride: two Hall-bars are shown for separate devices.

smaller than the PDMS cylinders. Reducing the areas contacted by the polymeric film makes the process more precise and preserves the integrity of the underlying heterostructure, upon which the handle is deposited. Handles are picked up at the standard temperature for BN, that is 40-45°, and they are deposited on the Hall-bar at 60°; the higher temperature makes the PPC less sticky and more fluid, thus reducing even more the risk of accidentally picking up the graphene-BN stack.
Since the handle needs to be perfectly on top of the graphene Hall-bar before proceeding, it can be moved using the AFM tip which pushes the handle from the side. Figure 2.9 shows the movement of handles into position on a device.

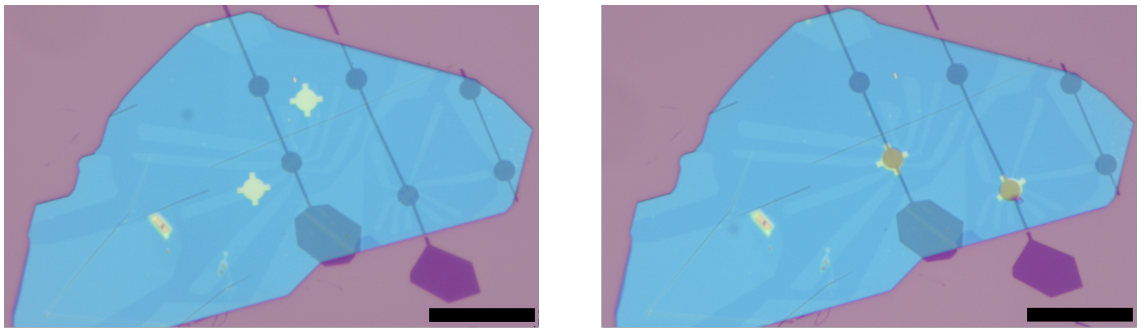

Figure 2.9: Handles deposited on the heterostructure: (a) before and (b) after moving with AFM. Scale bars reported on both images correspond to 20 μm.

After the handle has been deposited, a new step of electron beam lithography is necessary to place the contacts on the device; one contact is required per each extremity of the Hall bar and one for the gate, or two if the shape of the device allows it. The contacts terminate on the edges of the chip with square pads, which will be used to bond the chip to the holder (see 2.3).
Following the exposure and development of the resist, the metals are deposited through evaporation. The first deposition is a thin layer of titanium (Ti), 10 nm thick, which improves the adhesion to the SiO_2 substrate, followed by a 100 nm thick gold layer.

The metals are deposited uniformly on the substrate in the evaporator, and the pattern emerges after lift-off. This is done by placing the device in acetone overnight: the residual resist will detach from the chip, thus carrying away the metal deposited on top.
The aspect of the device after contact deposition is shown in figure 2.10.

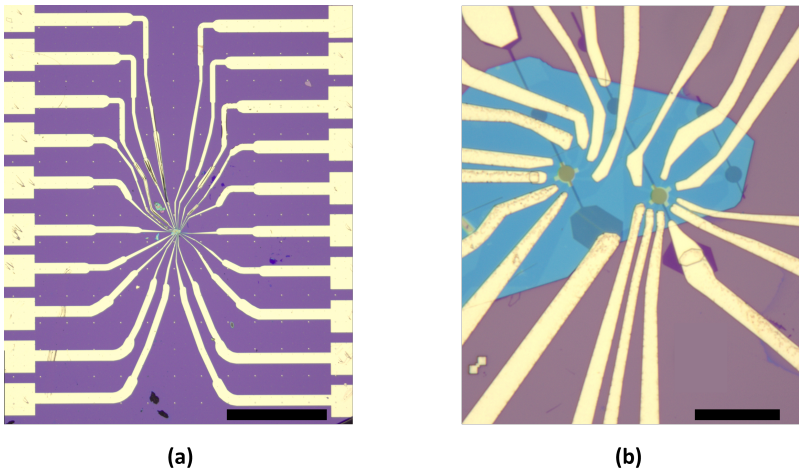

Figure 2.10: (a) Device with gold contacts and bonding pads (scale bar is equal to 1 mm) , and (b) zoom on the Hall-bar (scale bar is 20 μm).

2.3 Testing the contacts

The quality of the contacts is probed in a *probe station* using small conductive needles connected to a lock-in amplifier. The setup allows to extract the resistance of each contact by performing 2-Probe measurements. In such measurements two needles are put in contact each with a sample contact, so a current flows in the circuit completed by the graphene, connected to the contacts; it is possible to compute the resistance of such a path by measuring the voltage with the lock-in.
The resistance of a contact that's properly working is equal to a few kΩs; the measurements allow thus to find possible leaks between the contacts or the gate.

Once the contact performances have been assessed, the device can be placed on the holder. The holder is made of ceramics and presents a 2 mm thick highly conductive silicon chip on top to place the sample high enough for it to be reached with the AFM tip. The device chip is glued on it using conductive silver paste, to make a connection to the silicon bottom gate. The device contacts are wire bonded to the contacts on the holder, and the device is finally complete and ready for the electronic transport measurements.

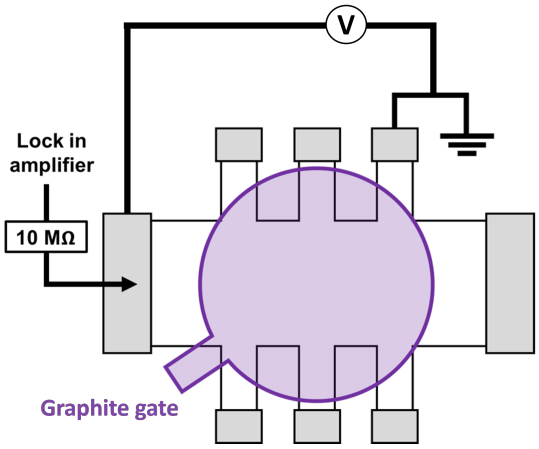

Figure 2.11: Schematic of the setup used to to a 2-Probe measurement.

Chapter 3

Moiré Measurements

The moiré effect on graphene can be probed by specific atomic force microscopy experiments, other than the electronic transport measurements; the object of such experiments is visualizing the hexagonal moiré pattern produced on the surface of graphene. This type of measurements can be performed on an heterostructure in which graphene is aligned with the bottom BN, and graphene is exposed. The moiré pattern produced in such devices is static and cannot be tuned: after the graphene flake is picked up, using the same procedure as section 2.2.2, it is difficult and not convenient to rotate it if the flakes are far from alignment.

Two kinds of AFM measurements can be used to probe the moiré: Piezoresponse Force Microscopy (PFM) and PeakForce mode.
PFM consists in contact mode measurements which are able to analyse piezoelectric materials by applying an alternating current between the tip and the sample: the inverse piezoelectric effect produces a deformation of the sample.
Such deformation is detected through the probe deformation using split photodiode detectors; then the signal is analysed through two lock-in amplifiers which monitor the vertical and lateral response respectively.[11]

On the other hand, PeakForce mode operates in non-contact conditions and the measurements are non-electric.
It is possible to analyse the interaction between tip and sample by Quantitative Nanomechanical Measurements (QNM): the topography of the sample is visualized through measurements of adhesion, Young modulus (DMT modulus) and deformation.
Deformation of the sample is caused by the pressure applied from the tip, whose maximum interaction force (peak force) is set and controlled by the user.
It is possible to visualize the moiré through these mechanical properties because, when such periodic potential is applied, the graphene lattice adjusts itself to follow the periodicity. Such phenomenon is defined as a commensurate state, and it is found when the flakes are close to full alignment, meaning the moiré periodicity is at least larger than 10 nm.
In the commensurate state, graphene stretches locally to reach an energetically favourable condition with respect to the vdW interactions with the underlying BN;

however, this behaviour is not extended to the whole flake but it is confined to *domains*, resulting in the formation of *domain walls* that accumulate the strain, separating the stretched areas from each other.
When the sample does not present good alignment, the commensurate state is not reached because it is not energetically favourable; therefore, a commensurate to incommensurate state transition can be observed on graphene as a function of the alignment angle with BN.[12]

The two techniques described were used to observe the moiré resulting from an aligned bilayer graphene-BN heterostructure; the moiré periodicity is around 14 nm, confirming that the stack is in full alignment. The heterostructure is shown in figure 3.1.

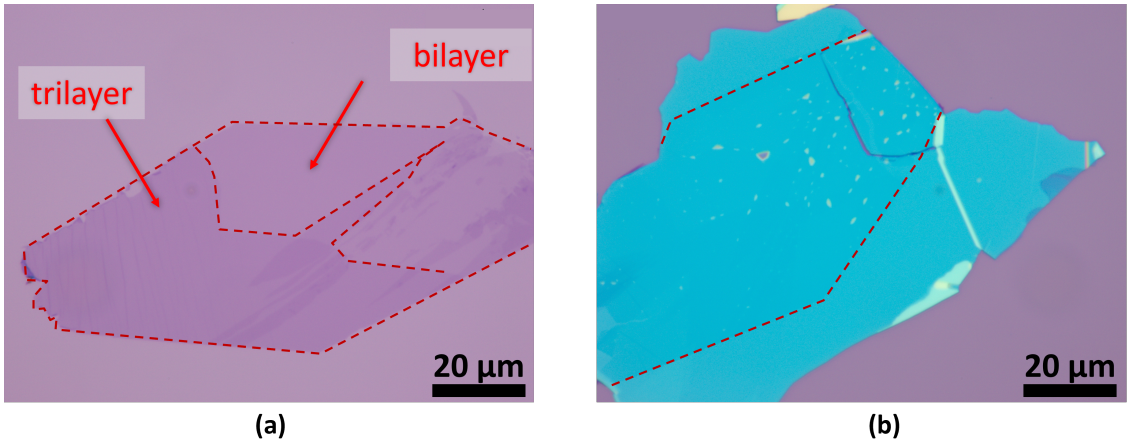

Figure 3.1: (a) Graphene flake containing areas with different layers. (b) Aligned graphene-hBN heterostructure, red dashed lines follow the border of the graphene flake.

Figure 3.2 shows the results obtained with PeakForce measurements, while the pictures in figure 3.3 were obtained through PFM experiments.

The pictures show that both techniques allow us to visualize the moiré; nevertheless, the images showing the best clarity are extracted from the PeakForce height sensor. In this case, the resolution could be improved possibly by choosing a different tip: tips are characterized by their radius and spring constant, and both parameters concur to the quality of the image via the interaction with the sample. In such a way also the DMT Modulus channel, so far showing a slight asymmetry, could be improved.

To further highlight the effectiveness of PeakForce mode, in figure 3.4 it is possible to see the moiré pattern in areas of the flake with a different number of layers.

Once again, the map of Young's modulus shows a slight asymmetry in the scanning direction: this is probably related to an enhanced friction and interaction between the tip and the sample as the latter is scanned.

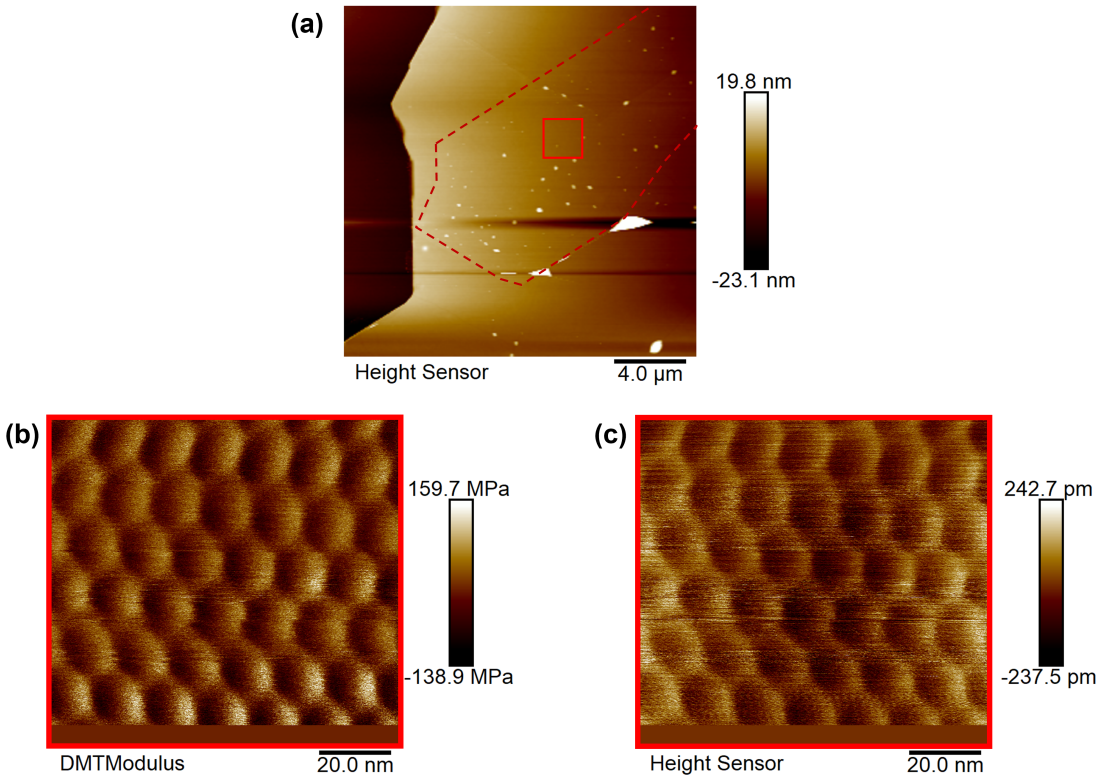

Figure 3.2: (a) Topography of the sample to analyse. (b) DMT Modulus and (c) height maps, showing the hexagons characteristic of the moiré pattern.

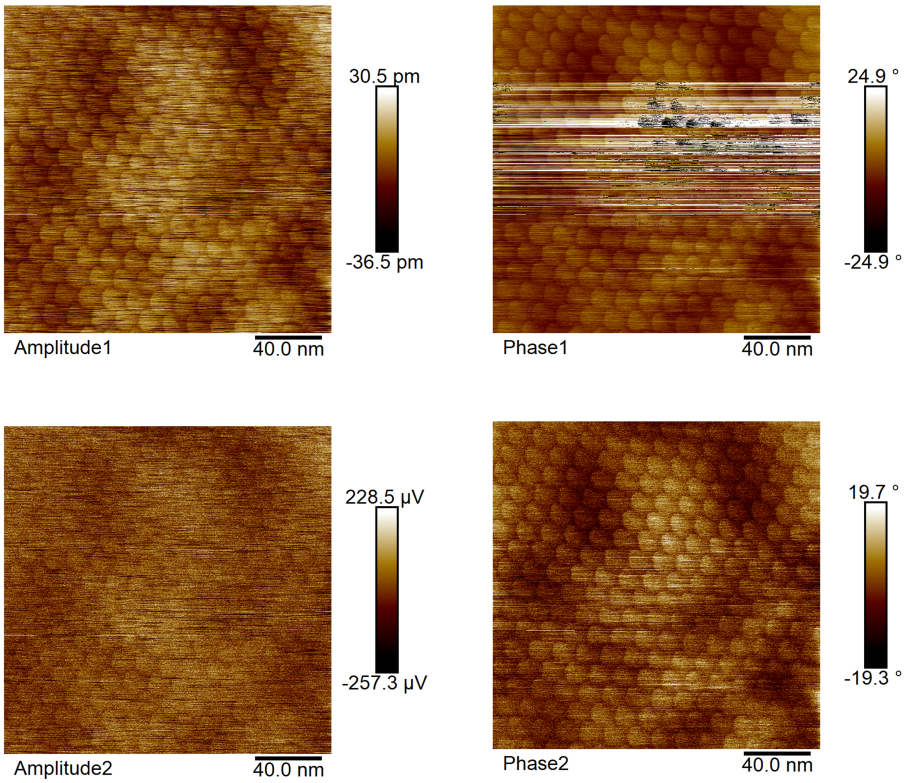

Figure 3.3: Amplitude and phase measurements from two lock-in amplifiers in PFM.

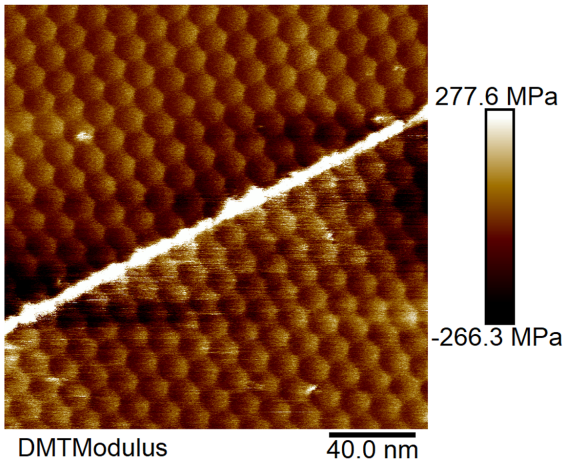

Figure 3.4: PeakForce large image (200 nm by 200 nm) including bilayer (left) and trilayer (right) areas of the graphene flake; both areas show the moiré pattern with 14 nm periodicity.

Chapter 4

Electronic Transport Measurements

4.1 Measurements Setup

Measurements of the dynamically rotatable device are performed inside the AFM at room temperature; the holder is electrically connected to lock-in amplifiers to perform 4-probe measurements.
A scheme of the setup for measurements is shown in figure 4.1. A constant current is injected in the device and then the voltage between two lateral contacts is measured to compute the resistance as the gate voltage V_g is swept.

Each measurement can be performed at a different angular alignment, which is

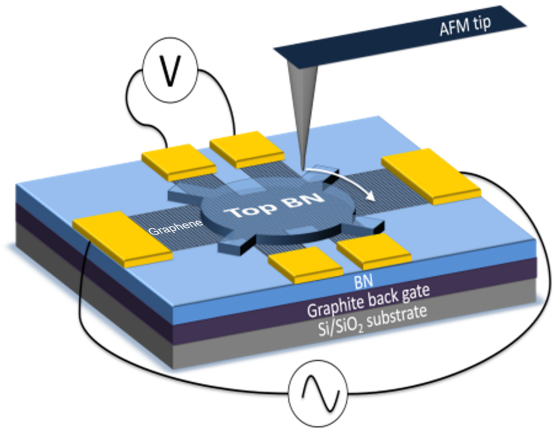

Figure 4.1: Setup of the four-probe measurement adapted from ref.[13]

tuned by rotating the handle with the AFM tip.
The first rotation is performed to find the alignment between the BN handle and graphene: when moving towards alignment the resistance at the charge neutrality point increases due to the opening of the energy gap. To observe this phenomenon it is necessary to fix the gate voltage at around -1 V, which is approximately the position of the main resistance peak; then the handle is rotated until the maximum value of the resistance is found.

4.2 Obtained Results

Measurements were performed on a single-aligned device, in which graphene is misaligned with respect to the bottom hBN, to understand its behaviour before measuring a double-aligned heterostructure. Two different alignment positions, shifted by 60° with respect to each other, are analysed on the device. Topography images taken with the AFM scan, figure 4.2, show the position of the handle on the Hall-bar in the aligned orientations.
Every time a measurement is performed a similar image is taken: this allows to determine the relative angle of rotation.

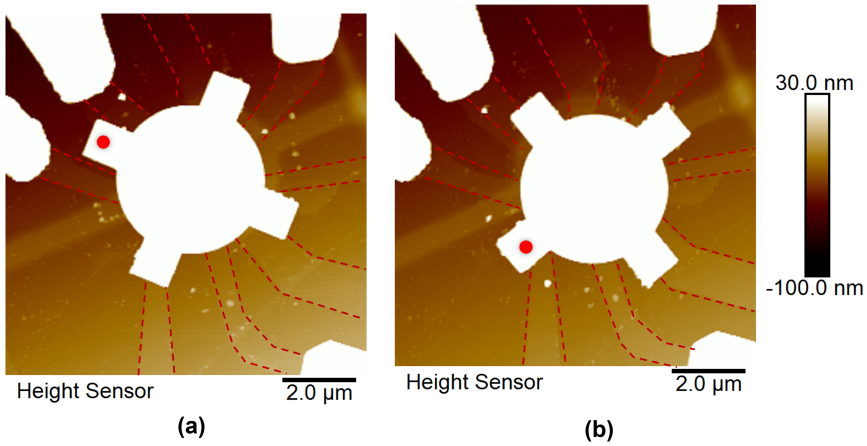

Figure 4.2: 0° (a) and 60° (b) aligned positions. The red dot has been drawn on the picture to highlight the rotation of the handle; the Hall-bar is defined by red dashed lines.

Figure 4.3 shows plots of the four-probe resistance R_{4P} as a function of the gate voltage V_g for 0° (a) and 60° (b) alignments. Measurements were taken in slightly misaligned positions and going towards alignment, to show the differences in the plots.
In fact, it is possible to observe the appearance of the satellite Dirac points in the form of secondary resistance peaks. Such peaks are much more remarked on the hole side (negative V_g values) because the modified band structure is electron-hole asymmetric.[6]
As the degree of alignment is increased, the secondary peak grows and its position gets closer to the charge neutrality peak.

Another effect of the alignment, as previously mentioned, is the increase of the resistance at the charge neutrality point.
This is better highlighted in figure 4.4: the height of the peak reaches a maximum at complete alignment, and symmetrically decreases when moving away from this position in either direction.
A peculiar phenomenon observed is that the intensity of R_{4P}^{CNP} is higher at what was defined as 60° alignment; these measurements were performed after the 0° alignment ones.

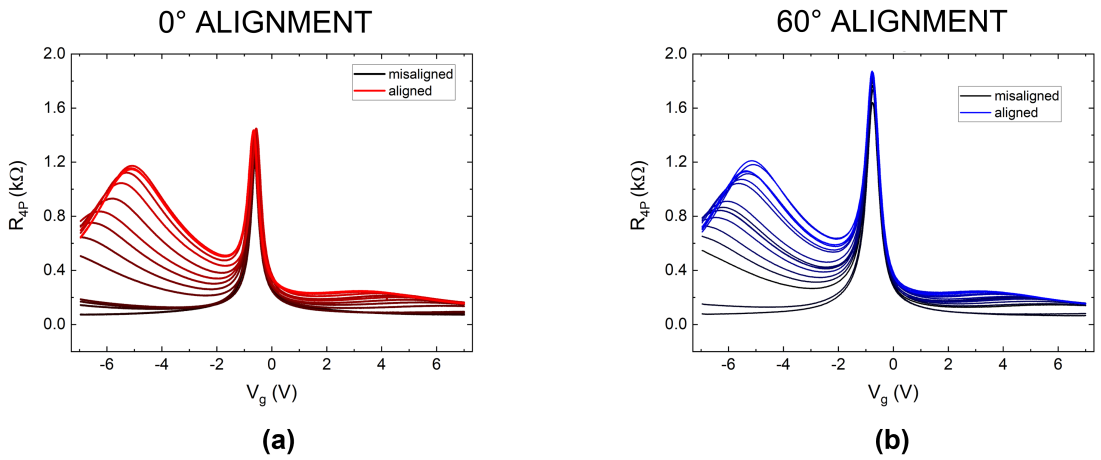

Figure 4.3: Four-probe resistance R_{4P} plots as a function of the gate voltage V_g for 0° (a) and 60° (b) alignments.

Although we don't have a precise explanation so far, we may attribute this to a different strain condition of graphene with respect to the BN orientation, or simply an improvement of the performances. Further measurements need to be performed to better understand the possible causes and whether this is a common phenomenon. For figure 4.4, and the following ones in this section, error bars on the angle value are related to the determination of the angular alignment from AFM images.

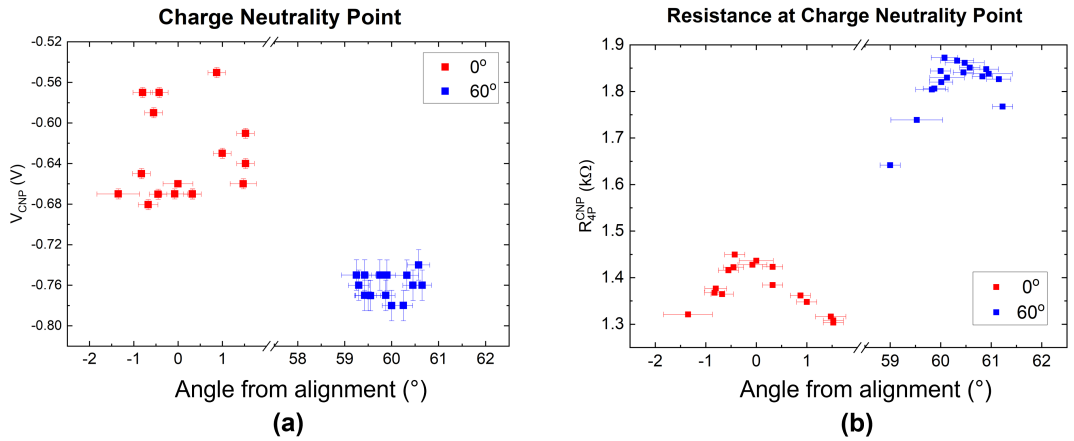

Figure 4.4: (a) Position of the Charge Neutrality Point V_{CNP} and (b) its four-probe resistance R_{4P} for different angles of alignment.

We can now analyse more in detail the satellite peak: similarly to the charge neutrality peak, also in this case the resistance reaches the maximum in a fully aligned condition. Contrary to the charge neutrality peak, here the resistance values corresponding to a range of ± 1° degrees from alignment are the same for 0° and 60°.
The position of the satellite peak V_{sat} also changes as a function of alignment,

becoming lower in absolute value when the device is fully aligned (figure 4.5).

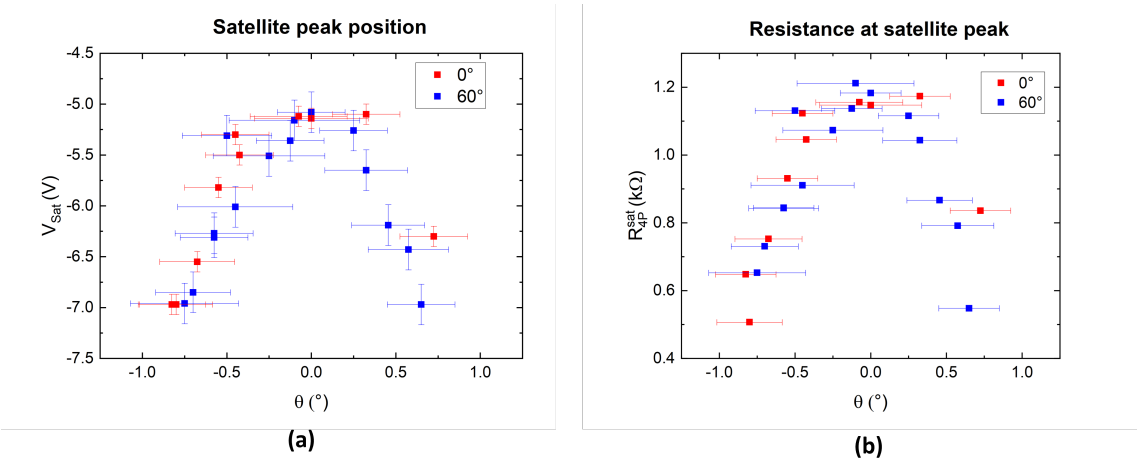

Figure 4.5: (a) Position of the satellite peak V_{sat} and (b) its four-probe resistance value R_{4P}^{sat} for different angles of alignment.

In the case of a double aligned sample,[8] both CNP and satellite peaks are not equal within 60° rotations of the top BN handle. The behaviour of the peaks is shown in figure 4.6, and it is 120° periodic. The main peak is maximum when the rotation between top and bottom BN layers is 0°, which corresponds to an enhancement of the inversion symmetry breaking (as explained in section 1.3), and it is reduced by 1 kΩ at 60° rotation. The same behaviour is observed for the secondary peak which is also maximum at 0° alignment; in this condition, the secondary peak is even higher than the main one.

The trend reported for double aligned samples in the literature is not the same

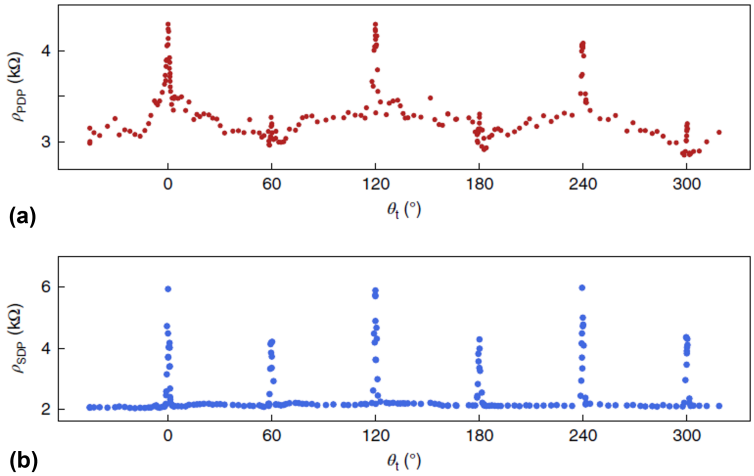

Figure 4.6: (a) Resistance peak at the CNP (b) satellite peak for different angles of alignment. Adapted from.[8]

as the single-aligned device examined. The main difference is that we report a

secondary peak of constant intensity, while only the intensity of the CNP changes.

The peaks related to the main Dirac point and the secondary ones are closer in the aligned state; it is possible to compute the difference of the respective voltages and plot it, as shown in figure 4.7.

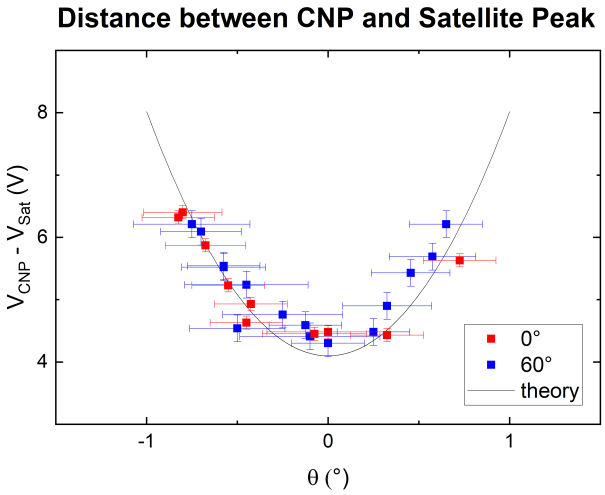

Figure 4.7: Distance (in V) between the main resistance peak and the secondary one for different angles of alignment.

The theoretical curve in figure 4.7 is plotted from the following equation:

$$V_{\text{sat}} - V_{\text{CNP}} = \frac{8}{C_{\text{g}}\sqrt{3}} \frac{2(1+\delta)(1-\cos\theta)+\delta^2}{(1+\delta)^2 a^2} \tag{4.1}$$

where δ is the lattice mismatch between hBN and graphene (0.018), a is the lattice constant of graphene (2.45 Å), θ is the relative rotation angle between the lattices, C_{g} is the capacitive coupling of the electrostatic gate.
C_{g} is actually computed as: $C_{\text{g}} = \frac{\epsilon\epsilon_0}{d}\frac{1}{e}$, where ϵ_0 is the vacuum permittivity, ϵ is the dielectric constant of boron nitride estimated to be about 4, e is the elementary charge and d is the thickness of the BN flake. For this device the height of the BN layer has been calculated through AFM measurements and is equal to 38 nm. The value of C_{g} is then 5.83×10^{15} V^{-1} m^{-2}.
Equation 4.1 is derived from the general relation between carrier density and gate voltage: $n = C_g(V_g - V_{\text{CNP}})$. Considering the carrier density at the satellite points, the expression becomes $n_{\text{sat}} = C_g(V_{\text{sat}} - V_{\text{CNP}})$.
Carrier density at full filling of the miniband is also computed as $n = \frac{8}{\sqrt{3}\lambda^2}$.
Replacing lambda with the equation 1.1, and substituting n_{sat} with the given expression, one finds the equation 4.1 for the theoretical curve.

Another interesting approach in visualizing the data consists in plotting the value of the satellite peak resistance as a function of the periodicity λ. In such a way a simpler correlation is made between the effect of the moiré superlattice and its size, as shown in 4.8. The period is computed for each value of θ as in equation 1.1.

Linear fits are reported for 0° and 60° alignments respectively, along with one of the overall data. Although error bars show that the data is not very precise after the different computations, the linear dependence of R_{4P}^{sat} is still visible. Moreover, the slopes of the computed fits are quite similar, confirming the validity of such an interpretation; the equations of the curves are $R^{sat} = 203.41\lambda - 1651.03$ for the 0° alignment, $R^{sat} = 193.07\lambda - 1454.94$ for 60° alignment, $R^{sat} = 192.04\lambda - 1480.69$ for the fit with both data combined.
These values are in agreement with the literature,[13] where $R^{sat} = 275.26\lambda - 2376$ for the same type of measurements, on single-aligned devices and at room temperature.

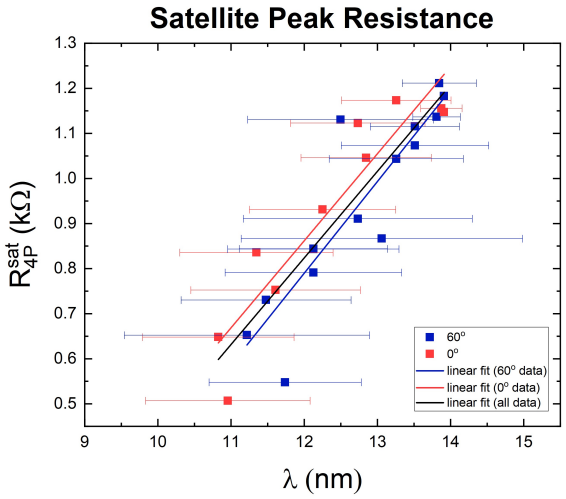

Figure 4.8: Dependence of the maximum value of the resistance at the satellite peak on the moiré periodicity λ.

As previously stated, all the data reported so far has been extracted from measurements of two different alignment positions shifted by 60°. The intention was to continue with measurements also for the consecutive alignment positions (i.e. 120°, 180°, and so on); this would allow us to give an explanation to the behaviour of the CNP observed in figure 4.4, for example whether this phenomenon could be related to a 60° periodicity.
Unfortunately this was not possible because a machine-related error in the AFM instrumentation caused the tip to collide on the device, thus breaking two contacts. Further characterization of the device was therefore impossible, and new devices are currently being built and measured, also aiming at a double-aligned configuration. The results are not yet available at the moment.

Chapter 5

Conclusions

The objective of this internship was to investigate the properties of double aligned graphene-hBN van der Waals heterostructures. Samples of dynamically rotatable heterostructures were produced through various steps involving different microfabrication techniques. Then, a technique using atomic force microscopy was implemented to visualize the moiré pattern of exposed graphene on hBN; this allows us to check whether the heterostructure that we have built can be effectively double aligned once the top alignment with the handle is achieved.
For the time being, one sample was characterized to investigate the effects of a moiré superlattice arising in a single-aligned heterostructure, in which graphene is not aligned to the bottom hBN layer; single-aligned devices are essential to understand the basic effect of the moiré superpotential on graphene. Two different alignment positions (shifted by 60°) were observed and characterized in the dynamically rotatable device, performing room temperature electronic transport measurements; such measurements allowed us to visualize resistance peaks which correspond to gaps opening in the electronic band structure of graphene, which is normally gapless. The trend which has been highlighted at the charge neutrality point in different aligned positions requires to complete measurements on new a device, which are still a work-in-progress at the moment.

The following step would be to investigate a double aligned device, which, as stated in precedence, is so far a relatively unexplored and certainly very interesting field of research. The interest is related to the many different effects that come from the enhanced moiré potential in the heterostructure, among which the finer tuning of the electronic properties of these materials. Moreover, other different phenomena are also being investigated around such heterostructures, among which ferroelectricity and the appearance of flat-band features in the electronic band structure,[8] which could certainly open the door to a wide range of applications in electronics.

Bibliography

[1] R. V. Gorbachev, J. C. W. Song, G. L. Yu, A. V. Kretinin, F. Withers, Y. Cao, A. Mishchenko, I. V. Grigorieva, K. S. Novoselov, L. S. Levitov, and A. K. Geim. Detecting topological currents in graphene superlattices. *Science*, 346(6208):448–451, 2014.

[2] C. R. Dean, A. F. Young, I. Meric, C. Lee, L. Wang, S. Sorgenfrei, K. Watanabe, T. Taniguchi, P. Kim, K. L. Shepard, and J. Hone. Boron nitride substrates for high-quality graphene electronics. *Nature Nanotechnology*, 5(10):722–726, Aug 2010.

[3] A. K. Geim and I. V. Grigorieva. Van der waals heterostructures. *Nature*, 499(7459):419–425, Jul 2013.

[4] A. H. Castro Neto, F. Guinea, N. M. R. Peres, K. S. Novoselov, and A. K. Geim. The electronic properties of graphene. *Reviews of Modern Physics*, 81(1):109–162, Jan 2009.

[5] Carlos Forsythe, Xiaodong Zhou, Kenji Watanabe, Takashi Taniguchi, Abhay Pasupathy, Pilkyung Moon, Mikito Koshino, Philip Kim, and Cory R. Dean. Band structure engineering of 2D materials using patterned dielectric superlattices. *Nat. Nanotechnol.*, 13:566–571, July 2018.

[6] Matthew Yankowitz, Jiamin Xue, Daniel Cormode, Javier D. Sanchez-Yamagishi, K. Watanabe, T. Taniguchi, Pablo Jarillo-Herrero, Philippe Jacquod, and Brian J. LeRoy. Emergence of superlattice dirac points in graphene on hexagonal boron nitride. *Nature Physics*, 8(5):382–386, May 2012.

[7] Pilkyung Moon and Mikito Koshino. Electronic properties of graphene/hexagonal-boron-nitride moiré superlattice. *Physical Review B*, 90(15), Oct 2014.

[8] Nathan R. Finney, Matthew Yankowitz, Lithurshanaa Muraleetharan, K. Watanabe, T. Taniguchi, Cory R. Dean, and James Hone. Tunable crystal symmetry in graphene–boron nitride heterostructures with coexisting moiré superlattices. *Nat. Nanotechnol.*, 14:1029–1034, November 2019.

[9] E. Arrighi, V. H. Nguyen, M. Di Luca, G. Maffione, K. Watanabe, T. Taniguchi, D. Mailly, J. C. Charlier, and R. Ribeiro-Palau. Non-identical moiré twins in bilayer graphene. *arXiv e-prints*, page arXiv:2205.01760, May 2022.

[10] P. Blake, E. W. Hill, A. H. Castro Neto, K. S. Novoselov, D. Jiang, R. Yang, T. J. Booth, and A. K. Gei. Making graphene visible. *Appl. Phys. Lett*, 91(063124), 2007.

[11] Leo J. McGilly, A. Kerelsky, N. R. Finney, K. Shapovalov, E. Shih, A. Ghiotto, Y. Zeng, S. L. Moore, W. Wu, Y. Bai, K. Watanabe, T. Taniguchi, M. Stengel, L. Zhou, J. Hone, X. Zhu, D. N. Basov, C. Dean, C. E. Dreyer, and A. N. Pasupathy. Visualization of moiré superlattices. *Nature Nanotechnology*, 15(7):580–584, Jul 2020.

[12] C. R. Woods, L. Britnell, A. Eckmann, R. S. Ma, J. C. Lu, H. M. Guo, X. Lin, G. L. Yu, Y. Cao, R. V. Gorbachev, A. V. Kretinin, J. Park, L. A. Ponomarenko, M. I. Katsnelson, Yu. N. Gornostyrev, K. Watanabe, T. Taniguchi, C. Casiraghi, H.-J. Gao, A. K. Geim, and K. S. Novoselov. Commensurate–incommensurate transition in graphene on hexagonal boron nitride. *Nature Physics*, 10(6):451–456, Jun 2014.

[13] Rebeca Ribeiro-Palau, Shaowen Chen, Yihang Zeng, Kenji Watanabe, Takashi Taniguchi, James Hone, and Cory R. Dean. High-quality electrostatically defined hall bars in monolayer graphene. *Nano Letters*, 19(4):2583–2587, Apr 2019.